Computers and Chemical Engineering 157 (2022) 107622

Contents lists available at ScienceDirect

Computers and Chemical Engineering

journal homepage: www.elsevier.com/locate/compchemeng

Optimal computer-aided molecular design of ionic liquid mixtures for post-combustion carbon dioxide capture

Andrea Silva-Beard [a], Antonio Flores-Tlacuahuac [b,*], Martín Rivera-Toledo [a]

[a] Departamento de Ingeniería Química, Industrial y de Alimentos, Universidad Iberoamericana Ciudad de México, Prolongación Paseo de la Reforma 880, Ciudad de México 01219, México

[b] Escuela de Ingenieria y Ciencias, Tecnologico de Monterrey, Campus Monterrey, Ave. Eugenio Garza Sada 2501, Monterrey, N.L, 64849, Mexico

ARTICLE INFO

Article history:
Received 11 September 2021
Revised 23 November 2021
Accepted 1 December 2021
Available online 8 December 2021

Keywords:
Multiobjective optimization
Ionic liquid mixture
Carbon dioxide capture
Mixed-integer nonlinear programming
Computer-aided molecular design

ABSTRACT

This work addresses the post-combustion carbon dioxide capture capabilities of optimally designed mixtures of ionic liquids, as well as pure ionic liquids. We postulate that ionic liquid mixtures can display better absorption rates and processing features when compared with pure ionic liquids. The computer-aided molecular design of the ionic liquids mixture was posed as a mixed-integer nonlinear programming problem to determine both the chemical structure and the amount of each ionic liquid in the mixture. Also, multiobjective optimization was performed to determine optimal operating conditions, specifically pressure and ionic liquids mixture feed stream, for an absorption separation process with various optimal mixtures. Results show that the anion [Tf_2N] with the chain -$(CH)_2(CH_2)_5(CH_3)_3$ was present both in the pure ionic liquid case and in the mixtures of these compounds. Results also indicate that, even though the amount of carbon dioxide absorbed by pure ionic liquid is slightly higher than the absorbed by ionic liquids mixture, there are important operational and environmental advantages of using such type of mixtures since they have milder physical properties than the pure ionic liquid.

1. Introduction

By-products of fossil fuels combustion are normally released into the atmosphere, increasing the concentration of greenhouse gases (GHG). Most organic and inorganic solvents used to selectively extract or separate them are highly toxic volatile organic compounds (VOCs) that can easily enter the atmosphere. Ionic liquids (ILs) have been proposed to replace VOCs. These liquids are formed by combining a cation and an anion. Normally the cation is a larger organic species than the anion, which is commonly an inorganic compound. An important characteristic of ILs is that their vapor pressure is practically zero, or at least very small, so they do not enter the atmosphere easily. Another advantage is that there are a wide variety of cations and anions that can be used to form ionic liquids and could be tailored for the different applications in which they are required (Niedermeyer et al., 2012). In addition, factors such as the level of toxicity, biodegradability, etc. could be imposed as desirable restrictions of the IL design, thus contributing to improve the sustainability characteristics of the industrial processes in which they are used.

Although there are some works dealing with the theoretical design of pure ILs for carbon dioxide (CO_2) capture (Chong et al., 2016; 2017; Gurkan et al., 2010; Hospital-Benito et al., 2020; Zhou et al., 2021; Zhang et al., 2021a; 2021b; Chemmangattuvalappil et al., 2020; Chen et al., 2019b; Palomar et al., 2019; Seo et al., 2020; de Riva et al., 2017), the effect of mixtures of ILs on the CO_2 capture performance has not been addressed in the open research literature. There may be some interesting and strong interactions that can be exploited for improving CO_2 removal from post-combustion streams. Those interactions are related to the chemical structure of the ionic liquids, mixture composition and the design parameters of the process where the CO_2 separation will take place. Here the hypothesis is that changes in the chemical structure of the compounds will have a deep effect on the operating processing parameters such as flowrates, temperature and pressure just to mention a few variables. On the other hand, operating conditions can also have a strong effect on the optimal chemical structure leading to improved performance. Some of the design methodologies proposed for addressing those interactions can be found elsewhere (Georgiadis et al., 2002; Valencia-Marquez et al., 2011; Molina-Thierry and Flores-Tlacuahuac, 2015; Chen et al., 2019a).

We postulate that better CO_2 capture can be achieved by allowing the chemical structure of ILs consider the presence of addi-

* Corresponding author.
E-mail address: antonio.flores.t@itesm.mx (A. Flores-Tlacuahuac).

https://doi.org/10.1016/j.compchemeng.2021.107622
0098-1354/

Nomenclature

Indexes

c	Component (CO_2, IL_1, IL_2)
i, p	Position of the functional group in the IL molecular structure
j	Number of valence
k, k_1, k_2	Type of functional group (see Table 2)
k_c	Type of anion-cation (see Table 1)
m	Maximum number of functional group type
s	Absorption stages

Greek variables

α	Variable in the Peng-Robinson EOS
η	IL viscosity
ϕ	Fugacity coefficient
Γ_k	Residual activity coefficient
Γ_k^c	Residual activity coefficient of group k in a solution with only type c molecules
γ_c	Activity coefficient of component c
γ_c^C	Combinatorial contribution to activity coefficient of component c
γ_c^R	Residual contribution to activity coefficient of component c
κ	Temperature function in density expression (Eq. (45))
ψ_{k_1,k_2}	Group interaction parameter between groups k_1 and k_2
ρ	IL density
θ_k	Auxiliar variable in UNIFAC model
υ_k	Valence number of the functional group k
Ω	Objective functions
ω	Acentric factor

Variables

A_p	Constant in Antoine correlation
A_z	Variable in the Peng-Robinson EOS
a_{k_1,k_2}	Interaction parameter between groups k_1 and k_2
B_p	Constant in Antoine correlation
B_z	Variable in the Peng-Robinson EOS
C_p	Constant in Antoine correlation
D_p	Constant in Antoine correlation
E_p	Constant in Antoine correlation
$f(\mathbf{x},\mathbf{y})$	Function of the continuous and binary variables
Fi_c	Auxiliar in UNIFAC model
$g(\mathbf{x},\mathbf{y})$	Inequality constrains
$h(\mathbf{x})$	Equality constraints
L	Liquid phase molar flow
L_{in}	Liquid phase molar feed
M	An arbitrary large number used in the chemical structure model
MW	IL molecular weight
m	Number of discrete binary variables
n	Number of continuous decision variables
n	Number of groups in an IL molecule
n_{max}	Maximum number of functional groups in an IL molecular structure
n_t	Total absorption stages
P	Operation pressure
P_c	Critical pressure
P^{sat}	Vapor pressure
Q_k	Group area parameter
q_c	Relative to molecular surface of pure component
R	Universal gas constant
R_k	Group volume parameter
r_c	Relative to molecular volume of pure component
S_{max}	Maximum valence number of a functional group
T	Operation temperature
T_b	Boling temperature
T_c	Critical temperature
T_m	Melting point temperature
T_r	Reduced temperature
V	Gas molar flow
V_c	Critical volume
V_{in}	Gas phase molar feed
V_{out}	Gas phase molar outlet
Vi_c	Auxiliar variable in UNIFAC model
vk	Number of bonds per functional group
X	Domain of continuous variables $\mathbf{x}$
X_{k_1}	Fraction of group k_1 in the mixture
$\mathbf{x}$	Continuous decision variables
x_c	Mole fraction of component c in the liquid phase
$\mathbf{y}$	Binary decision variables
y_c	Mole fraction of component c in the gas phase
Z_v	Compressibility factor for the vapor phase in the Peng-Robinson EOS

Binary variables

$u_{i,k}$	Position i of group k in the IL molecule
w_i	Auxiliar variable in the MINLP model
$z_{i,j,p}$	Bond between functional groups i and p in the valence j of the functional group i

tional sets of cations and anions. This idea is intuitively appealing since it can be linked to introducing additional degrees of freedom in the ILs design process. Moreover, the proportion or mass of individual ILs provides an additional degree of freedom to further improve CO_2 capture, when considering mixtures of ILs. Finally, operating conditions (temperature, pressure, and flow rates profiles) were also considered as decision variables since they can have a strong impact on CO_2 capture performance.

These are the main factors, (i.e., chemical structure, mass of individual ILs and operating conditions) that we address in this work to advance in the potential reduction of GHG entering the atmosphere. By not using VOCs, the degree of sustainability of the CO_2 capture process will increase. It should be stressed that, with proper changes, the same theoretical framework can be used to capture additional GHG such as methane, nitrogen oxides (NO_x) and sulphur.

Theoretical design of chemical products can be achieved through experiments, databases, heuristics, or model-based models (Zhang et al., 2020). Model-based methods comprise quantum mechanics (QM), molecular dynamics (MD), Density Functional Theory (DT), group contribution (GC) methods, thermodynamic models, Population-based model (PBM), Computational fluid dynamics (CFD), and process simulation approaches (Zhang et al., 2020). Computer-aided molecular design (CAMD) is a computational approach to design a molecular structure, frequently completely novel, that combines molecular modeling techniques, thermodynamics, and numerical optimization (Austin et al., 2016). CAMD problems determine the molecular structure that complies with specific target properties for a certain application (Gani, 2004) and have been widely used to determine optimal chemical structures (Chong et al., 2016; 2017; Gurkan et al., 2010; Chen et al., 2018; Karunanithi and Mehrkesh, 2013; Hada et al., 2015; Chen et al., 2019a). In general, the CAMD approach is less computationally demand in comparison to theoretical DFT strategies. Ideally a novel compound can be designed by CAMD optimization formulations, whereas later some theoretical properties (i.e. chemical stability

of the compound) can be assessed by rigorous DFT calculations. We have applied this compound design plus validation approach in a recent work dealing with the design of lubricants (Valencia-Marquez et al., 2021). Moreover, new approaches to molecular design, based on the use of advanced data-driven deep learning techniques such as Auto-Encoders and Generative Adversarial Networks (Ramsundar et al., 2019), deserve to be considered in the search for new sustainable compounds.

In this work, the theoretical design problem of ILs mixtures, both chemical structure and amount of each IL, was posed as a Mixed-Integer NonLinear Programming (MINLP) problem. For the formulation of the optimization problem, physical absorption mechanisms were considered. CAMD was used, with GC methods to predict the product physical properties, and thermodynamic models to predict activity coefficients. Due to the enormous number of potential ILs, setting the problem of design of the ILs as an optimization problem will allow a more rational search for the product that complies with the desired design characteristics, without having to experimentally examine a wide range of possible cation-anion combinations.

The variables that were determined throughout the development of the project were: (1) structure of ionic liquids (cation-anion binomial) in the mixture, (2) physical properties of ionic liquids, (3) composition of the ionic liquids mixture (% of each IL in the mixture), (4) % of CO_2 absorbed and (5) operating conditions of the equipment (pressure, temperature and liquid and gas flow rates). The CO_2 capture process was assumed to take place in a single and two stage process. The best operating conditions for a given IL mixture in a two stage absorption system, specifically pressure and ionic liquids mixture feed, were determined through Pareto diagrams. These are multiobjective optimization problems, given that these two variables change in opposite directions. Moreover, pressure and ionic liquid inlet flowrate have a direct impact in the process energy consumption. Regarding diffusivity, in this work we assumed that the modeling of the absorption tower, where separation takes place, can approximate that of a tower of plates and that each plate is in equilibrium, so the determination of the diffusivity was not necessary. Moreover, it should be stressed that in the present work no attempt to address the impact of uncertainty in the resulting ILs design and performance was made. One of the main drawbacks and uncertainty related to the design of ILs has to do with the availability of reliable physical and thermodynamic information, which can be tackled through the use of probabilistic machine learning methods such as bayesian neural networks (Murphy, 2012).

Finally, we would like to stress that the methodology used in this research is rigorous and the results are novel. To our knowledge, no work has been published regarding IL mixture optimal design for CO_2 capture or multiobjective optimization of the absorption operation conditions and for different optimal designed IL mixtures. The intend of our work was not to propose a new CAMD or MINLP method. Our objective was to obtain better CO_2 capture capabilities using IL mixtures. Our findings show that using IL mixtures give important operational advantages versus using pure IL while having similar absorption rates, which do link to overall absorption efficiency (i.e., energy consumption due to smaller quantities of IL in the feed stream). We think this finding is a relevant and novel contribution.

2. Background

Industrial gas emissions include CO_2, NO_x, carbon monoxide, suspended particles, and sulfur dioxide, and virtually all of them are GHG. These emissions are harmful to humans, agriculture, forests, various ecosystems, and the environment in general as they increase the greenhouse effect on our planet and therefore can contribute to climate change (Rahman et al., 2017). The correlation between the increase in the concentration of CO_2 in the atmosphere and the greenhouse effect has started a worldwide debate aimed at reducing emissions of CO_2 and other GHG (Ramdin et al., 2012).

GHG emissions are made up of 77% CO_2 (Rahman et al., 2017). Carbon dioxide emissions have had a significant increase since the beginning of the industrial revolution. Human activities (industry, population, etc.) have been identified as the main cause for increasing the concentration of CO_2 in the atmosphere from approximately 280 ppm before industrialization to current levels of 420 ppm (Ramdin et al., 2012). It remains as a pending task to prove the veracity of this statement. Meanwhile, for sustainability reasons, it is important to reduce the amount of GHG entering the atmosphere. There are various works establishing that the concentration must be below 350 ppm for there to be a safe environment for humans (Rahman et al., 2017). Global CO_2 emissions in 2008 were 29.4 gigatons (Gt), which implies an increase of approximately 40% compared to the 20.9 Gt in 1990 (Ramdin et al., 2012).

Currently the power sector is responsible for 41% of CO_2 emissions from the energy sector, followed by the transportation sector (23%) and the construction sector (10%), among others. The highest proportion of CO_2 emissions in the energy sector is related to the combustion of fuels to generate electricity or heat. In 2008, CO_2 emissions generated using coal as fuel represented 43%, using oil 37% and gas 20%. Although new forms of power generation are being explored, seeking a transition from fossil fuels to low-carbon technologies, in the medium-term solid fuels, particularly coal, will continue to form an important part of the power generation portfolio (Ramdin et al., 2012).

A certain amount of CO_2 in the atmosphere is necessary to absorb thermal radiation from the earth surface. The greenhouse effect is important to maintain the temperature of the earth in suitable conditions for life. However, too many GHG can cause a drastic increase in the temperature of the earth that can strongly affect the entire ecosystem. Therefore, it is important to focus efforts on the control of CO_2 emitted and to promote sustainable practices in the industrial sector aimed at reducing the production of this gas.

Large-scale CO_2 capture and storage is considered one of the most promising ways to mitigate GHG emissions (Zhang et al., 2012). Although it could be seen as a temporary solution, carbon capture and storage are undoubtedly essential to solving the problem. Both capture and storage are technically complex and there are many obstacles to overcome in making them commercial processes. The main obstacle is the energy cost associated with the separation (Ramdin et al., 2012). In this work we only address the problem related to the capture of CO_2.

Processes used to capture CO_2

One of the most important technologies that can be used to reduce CO_2 emissions to the atmosphere is carbon capture and storage (or sequestration) (CCS) which is defined as the removal of CO_2 directly from industrial plants and their subsequent storage in a safe environment. The three main separation processes for CO_2 capture are (1) absorption, (2) adsorption and (3) membrane systems, and can involve the use of a post-combustion, pre-combustion or oxyfuel capture systems (Rahman et al., 2017). Chemical and physical absorption are the most intensively processes for CO_2 capture. In this project we focused on a post-combustion absorption separation system.

One of the most used industrial procedure for the capture or recovery of various types of gases consists of the absorption of such gases by liquids, commonly called solvents. For a given gas to be absorbed by a solvent, several requirements must be met:

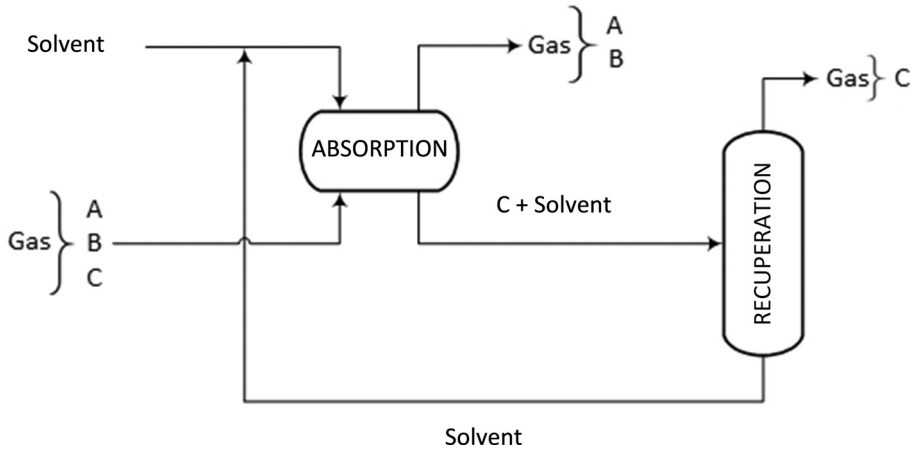

Fig. 1. Absorption process.

(a) chemical affinity between the gas and the solvent (measured through combination reactions so that the absorption can be physical, chemical, or a combination of both) and (b) appropriate operating conditions, assuming the above requirement is met.

A typical flow diagram of a solvent gas absorption process is shown in Fig. 1. However, in this project only the absorption part of the process was considered.

The process consists of two main steps:

(1) In the absorption phase, the gas (in Fig. 1 consists of 3 hypothetical components A, B and C, where the compound to be absorbed or recovered is component C) comes into contact with the solvent. The products of this phase are a gas that mainly contains components A and B, and a stream of solvent enriched with the captured compound C.
(2) In the recovery phase the captured gas is separated from the solvent. Since solvents are commonly expensive compounds, it is customary to recover and recycle as much of these materials as possible. However, solvents tend to lose their efficiency as capture or recovery agents over time and with use, so at some point must be replaced by new solvents.

Generally, of the two steps described above (absorption and recovery), the recovery step is the one that requires the greatest use of energy to carry out the process of separating the recovered gas and the solvent. One way to reduce the energy consumption of this phase is to use optimal operating conditions aimed at minimizing such energy consumption. Even though in this project we did not consider the recovery step, minimizing the IL mixture feed stream will result in less energy consumption in that part of the process. A similar effect will be obtained by minimizing the system operation pressure. In the present work we concentrate in the design of ionic liquid mixtures aiming at achieving acceptable rates of CO_2 capture targets. The introduction of the regeneration unit will force to consider the economic optimization, besides the design of the optimal mixture and underlying ionic liquids, of the integrated process. Maximizing CO_2 recovery and minimizing ionic liquids flowrates can be achieved at this level and it leads to an multiobjective optimization problem. To avoid additional complex behaviour, in this work we concentrate in just the design of the ionic liquids and their mixtures and leave for future work the introduction of the regeneration unit and economic optimal design issues. In addition to demanding large amounts of energy for their operation, gas capture processes using solvents present sustainability problems and health risks. Many of the most common industrial solvents (e.g., benzene, toluene, cyclohexane, etc.) have high vapor pressures so they easily evaporate and enter the atmosphere. Because some of these compounds present serious risks to health and the environment (carcinogenic compounds), it is essential to develop new types of solvents that are: (a) economical in their production, (b) non-toxic, (c) easy to recover and/or (d) capable of capturing as much of the gas in question as possible. Clearly, the ideal scenario is to be able to develop solvents that comply with all requirements, but this is not always feasible. For instance, ionic liquids may satisfy requirements (b), (c) and (d), but hardly (a) since currently their production is more costly than organic solvents.

Capturing CO_2 from post-combustion process flue gases is the biggest challenge due to the large volume, low CO_2 concentration, and low pressures. Since the energy consumed in the capture of CO_2 represents approximately $^2/_3$ of the total energy used in the carbon capture and storage processes, the development of processes of lower energy consumption plays a very important role (Zhang et al., 2012).

CO_2 capture using amines

Currently the technology available for the capture of CO_2 is based on the use of amines as solvents, such as monoethanolamine (MEA). The separation flowsheet for CO_2 capture using amines is similar to the one displayed in Fig. 1. The energy consumption to remove a ton of CO_2 using a 30% MEA aqueous solution assuming a removal of 90% CO_2 is estimated between 2.5 and 3.6 Gigajoules (GJ). The minimum theoretical work to separate and compress CO_2 to 150 bar is 0.42 GJ/ton CO_2, indicating that there is significant potential for process improvement (Ramdin et al., 2012). A recent work aimed to the optimization of the traditional amines CO_2 capture process using rigorous models has been reported elsewhere (López-Bautista and Flores-Tlacuahuac, 2020).

CO_2 capture using ionic liquids

Industrial processes that use some type of solvent to capture CO_2, tend to require large amounts of energy and usually display health problems when they enter the atmosphere (Sreedhar et al., 2017). This has led to the search for other solvents to be used in the capture of CO_2 by absorption (Zhang et al., 2012). There is enormous potential for the discovery and application of new materials that offer significant improvements to the way we generate, store, and distribute energy. Ionic liquids are a family of materials in that category that can be explicitly designed to meet a certain need or use. Such compounds are formed by the combination of anions and cations and have been used in diverse applications (MacFarlane et al., 2014; Seddon, 1997; Lei et al., 2017; Plechkova and Seddon, 2008). As liquid salts, dominated by electrostatic forces between their ionic molecules, the key properties

of certain components offer very low volatility/flammability and high chemical and electrochemical stability. That makes them potentially ideal solvents and electrolytes (MacFarlane et al., 2014).

One of the main advantages of ILs for capturing CO_2 is that they have almost negligible vapor pressure and thus there would be no contamination of gas streams and no negligible loss of ionic liquid. The low vapor pressure also translates into lower energy consumption in the stripper and in solvent regeneration. Through simulations it is estimated that the capture of CO_2 using the ionic liquid [bmin] [Ac] can reduce energy losses by 16% compared to the commercial process using MEA. An investment of the process with IL is estimated 11% lower than the processes with MEA and that would provide a 12% reduction in the carbon footprint caused by the equipment. Energy savings between 12 and 16% have also been reported by using a 60% IL mixture with water (Zhang et al., 2012).

Although many research efforts have been made in the identification of new solvents such as mixed amines, biphasic solvents, amines with structural modifications, ionic liquids with specific characteristics, there is still a great scope for expanding the most effective solvents from an operational, economic, and environmental point of view. Solvents with desired attributes of solubility, low regeneration energy, mass transfer, kinetics, and thermodynamics, biodegradability, low toxicity, low viscosity, and therefore better transport properties, as well as better chemical and thermal stabilities, need to be developed (Sreedhar et al., 2017).

It is important to emphasize that research on the capture and removal of CO_2 with IL solvents is relatively new (Senftle and Carter, 2017) and many of the effects and issues have not been studied or understood well enough to meet industrial needs. Therefore, more studies on the subject are required to drive industrial innovation and achieve commercial viability of CO_2 separation technologies with ILs (Sreedhar et al., 2017).

3. Problem definition

There are some reports (Aghaie et al., 2018; Sistla and Khanna, 2014; Torralba-Calleja et al., 2013; Lotto et al., 2021; Avila et al., 2021) indicating the advantages of post-combustion CO_2 capture using ionic liquids. However, most of the reported studies are only related to pure ionic liquids. An interesting extension of those works would be to address the effect of mixtures of ionic liquids on CO_2 capture performance. Moreover, an additional degree of freedom to be taken into account would be the composition, or proportion, of the ionic liquids. Some other aspects, such as exploiting the interaction between chemical structure and process design (Valencia-Marquez et al., 2011; Sakizlis et al., 2004) have been taken into account as well. Implicit in these comments is the following hypothesis to be tested in the present work:

Hypothesis: A mixture of optimally designed ionic liquids (i.e. featuring both chemical structure, composition and a set of processing parameters) will be able to capture larger amounts of post-combustion CO_2 process stream compared to similar single ionic liquids capture systems.

Hence, the problem addressed in this work can be defined as follows:

- Given is a fixed-point post-combustion polluted stream, featuring CO_2 and other pollutants, from which CO_2 ought to be captured such that a free CO_2 high-purity stream is manufactured. To realize the high-purity separation process an absorption process stream, composed of a mixture of ionic liquids, will be used. Hence, the central problem in the present study consists in obtaining the optimal chemical structure design of a mixture of ionic liquids (IL) to capture CO_2, the optimal composition of such a mixture as well as optimal processing operating conditions such that maximum CO_2 capture is achieved.

Table 1
Cations and anions used to define the ILs structures.

Ion	Name
Cations:	
R–[mIm]$^+$	Methylimidazolium
R–[mPy]$^+$	Methylpyridinium
R–[mPyr]$^+$	Methylpyrrolidinium
R–[P_{222}] $^+$	Triethylphosphonium
Anions:	
[$DMPO_4$]$^-$	Dimethylphosphate
[TFA]$^-$	Trifluoroacetate
[BF_4]$^-$	Tetrafluoroborate
[TfO] $^-$	Trifluoromethanesulfonate
[Cl]$^-$	Chloride
[PF_6]$^-$	Hexafluorophosphate
[Tf_2N]$^-$	Bis(trifluoromethylsulfonyl)-imide
[$MeSO_4$]$^-$	Methylsulfate
[$EtSO_4$]$^-$	Ethyl sulfate
[$DEPO_4$]$^-$	Dimethyl phosphate
[$MDEGSO_4$]$^-$	2-(2-methoxyethoxy)ethyl sulfate
[NO_3]$^-$	Nitrate
[SCN]$^-$	Thiocyanate

Table 2
Functional groups used to define –R chain of the ILs structures.

Code	Functional group	Number of bonds
1	$-CH_3$	1
2	$-CH_2-$	2
3	>CH–	3
4	–OH	1
5	$-CH_3CO$	1

The system consists of a 100% CO_2 gas feed at 303.15 K and 30 bars (conditions taken from a previous work of our research group (Valencia-Marquez et al., 2017)). It is assumed that the pure CO_2 gas stream is obtained by a previous process in which the rest of the post-combustion flue gas components (mainly N_2) are separated. The cations and anions used in the present work are presented in Table 1 and the functional groups that can be added to the main cation are presented in Table 2. These cations and anions were selected based on our group previous work (Valencia-Marquez et al., 2017), but we added some anions (specifically nitrate) and some other cation skeletons (specifically methylpyridinium, methylpyrrolidinium and triethylphosphonium) based on published data on CO_2 capture (Ramdin et al., 2012). Even though in this work we used some information and experience of our previous work, there are important differences. In first instance, in Valencia-Marquez et al. (2017) the equilibrium was determined by an empirical correlation developed by Mortazavi-Manesh et al. (2011) while in this work we used UNIFAC to determine the activity coefficients of the compounds at the equilibrium. Secondly, as mentioned earlier, we incorporated some other cations that are considered less environmentally hazardous (Abramenko et al., 2020).

To predict physical properties or activity coefficients through group-contribution methods, the IL molecule has to be separated into different functional groups (see Fig. 2). In this regard, there are three ways to decompose an ionic liquid (Taheri et al., 2018):

1. The IL molecule is decomposed into several groups: one anion group (e.g. $MeSO_4$, element 3 of Fig. 2), one main cation group (e.g., methylimidazolium, element 1 of Fig. 2) and the other functional groups in –R (e.g. -CH_2 or -CH, element 2 of Fig. 2).

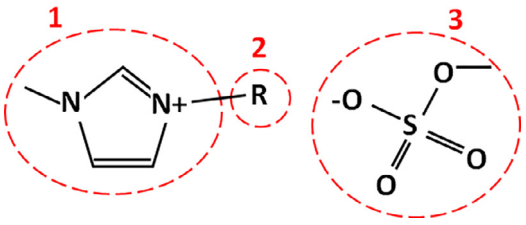

Fig. 2. Constituents of an ionic liquid molecule.

2. The IL molecule is separated into two types of functional groups: cations (elements 1 and 2 of Fig. 2) and anion (element 3 of Fig. 2).
3. The IL molecule is divided into several groups that are electrically neutral, that is, one group has the anion and the skeleton of the main cation (elements 1 and 3 of Fig. 2) and the rest of the groups present on the cation side (element 2 of Fig. 2).

In this work, as in Taheri et al. (2018), we adopted the third approach to decompose the IL molecule due to the very strong electrostatic interaction between cation and anion (Dong et al., 2020a) and UNIFAC data availability.

The terminology we used in this work to present a specific resulting –R chain consists on indicating the quantity of each functional group in the chain structure, shown in the position indicated in the code column of Table 2. For example, the chain CH_3-CH_2-CH_2-CH_2-CH_2– would be represented by "-14" because it has one -CH_3 (first position of the code) and four -CH_2 (second position of the code) functional groups. To indicate a specific IL molecular structure we used the notation [cation][anion]–R. For example, an IL with a molecular structure with a methyl imidazolium cation, a tetrafluoroborate anion and CH_3-CH_2- in the –R chain, would be presented as [mIm][BF4]-11.

4. Optimization formulation

The Computer-Aided Molecular Design (CAMD) model is defined as a Mixed-Integer NonLinear Programming (MINLP) problem. The model builds a molecular structure of an ionic liquid from the elements shown in Tables 1 and 2. A typical MINLP problem is characterized by an objective function Ω subject to equality and inequality constraints. The general formulation is as follows:

$$\min_{\mathbf{x},\mathbf{y}} \ \Omega(\mathbf{x},\mathbf{y}) = f(\mathbf{x},\mathbf{y})$$

s.t.

$$g(\mathbf{x},\mathbf{y}) \leq 0$$
$$h(\mathbf{x}) = 0$$
$$\mathbf{x} \in X, \ \mathbf{x} \in \Re^n$$
$$\mathbf{y} \in \{0,1\}^m$$

Typically, equality constraints $h(\mathbf{x})$ represent process conservation equations, physics of the phenomena and/or physical and thermodynamic properties calculation, i.e. density estimation. Inequality constrains $g(\mathbf{x},\mathbf{y})$) commonly are used to set bounds on decision variables, i.e. melting point has to be lower than the operating temperature. Moreover, $\Omega(\mathbf{x},\mathbf{y})$ stands for the target objective function. As usual, the $\Omega(\cdot), g(\cdot)$ and $h(\cdot)$ functions are assumed to be Lipschitz functions. The $\mathbf{x}$ vector stands for a continuous variable used to represent properties or any other continuous unknown variable, whereas the $\mathbf{y}$ vector refers to binary variables used for the selection of the best molecular design. Finally, n stands for the number of continuous decision variables, whereas m is the number of discrete binary variables.

In this work, three different optimization problems were tackled: 1) the CAMD of a pure IL that captures the most CO_2, 2) the CAMD of a binary ILs mixture and each IL composition, that captures the most CO_2, and 3) the operation conditions, particularly the ILs mixture feed stream and operation pressure of a two stage absorption separation process. Inequality constraints are associated to the selection of the functional groups, i.e. the design of the molecule, whereas equality constraints are used for the estimation of physical and thermodynamic properties. Optimization calculations in this work were performed with the GAMS software Release 31.1.1.

4.1. Pure ionic liquid design

Objective function

The objective function for the pure ionic liquid CAMD problem is given by:

$$\max_{\mathbf{x_1},\mathbf{y_1}} \ \Omega_1 = x_{CO_2} \tag{1}$$

where x_{CO_2} is the carbon dioxide mole fraction in the liquid phase and $\mathbf{x_1}$ and $\mathbf{y_1}$ are the continuous and binary decision variables related to the MINLP problem.

Constraints

The pure IL design optimization problem is subject to three sets of constraints: (1) chemical structure of the ionic liquid defined by Eqs. (2)–(19), (2) physical equilibrium given by Eqs. (20)–(39) and (3) ILs physical properties bounds defined by Eqs. (49)–(54).

Chemical structure

The chemical structure model constraints for the ionic liquid were obtained from Churi and Achenie (1996) and Valencia-Marquez et al. (2017) and are as follows.

Eq. (2) establishes the maximum structural groups per molecule of IL:

$$\sum_{i}^{n_{max}} \sum_{k}^{m} u_{i,k} \leq n_{max} \tag{2}$$

Eq. (3) is the implementation of the octet rule:

$$\sum_{p}^{n_{max}} \sum_{j}^{S_{max}} z_{i,j,p} = \sum_{k}^{m} u_{i,k} \upsilon_k \qquad i = 1 \ldots n_{max} \tag{3}$$

Eqs. (4)–(7) are to ensure that only one molecule is formed:

$$\sum_{p}^{i-1} \sum_{j}^{S_{max}} z_{i,j,p} \geq -w_i \qquad i = 2 \ldots n_{max} \tag{4}$$

$$\sum_{i}^{n_{max}} \sum_{k}^{m} u_{i,k} + \sum_{i}^{n_{max}} w_i = n_{max} \tag{5}$$

$$w_1 = 1 \tag{6}$$

$$w_i \leq w_{i+1} \qquad i = 1 \ldots (n_{max} - 1) \tag{7}$$

Eq. (8) assures that each functional group in a linear molecule contributes with only half bond:

$$\sum_{i}^{n_{max}} \sum_{k}^{m} u_{i,k} \upsilon_k = n - 1 \tag{8}$$

Eq. (9) is included to account for different valencies of the groups:

$$\sum_{j=\upsilon_k}^{S_{max}} \sum_{p}^{n_{max}} z_{i,j,p} - \sum_{p}^{n_{max}} z_{i,\upsilon_k,p} + M u_{i,k} \leq M \qquad i = 1 \ldots n_{max}, k = 1 \ldots m \tag{9}$$

Eq. (10) is a symmetry restriction:

$$\sum_{j}^{S_{max}} z_{i,j,p} = \sum_{j}^{S_{max}} z_{p,j,i} \qquad i = 1 \ldots (n_{max} - 1),\ p = (i+1) \ldots n_{max} \tag{10}$$

Eq. (11) is to ensure that a given group can be attached at the most to another group:

$$\sum_{p}^{n_{max}} z_{i,j,p} \leq 1 \qquad i = 1 \ldots n_{max},\ j = 1 \ldots S_{max} \tag{11}$$

Eq. (12) establishes that the ith group exists if the $(i-1)$th exists:

$$\sum_{k}^{m} u_{i,k} - \sum_{k}^{m} u_{i-1,k} \leq 0 \qquad i = 2 \ldots n_{max} \tag{12}$$

To ensure that only one group k is in the position i:

$$\sum_{k}^{m} u_{i,k} \leq 1 \qquad k = 1 \ldots m \tag{13}$$

To ensure that only one group is not attached to itself:

$$\sum_{j}^{S_{max}} z_{i,j,p} = 0 \tag{14}$$

Only one anion-main cation has to be selected:

$$\sum_{k_c} u_{1,k_c} = 1 \tag{15}$$

Eliminate multiple bonds:

$$\sum_{j}^{S_{max}} z_{i,j,p} \leq 1 \tag{16}$$

Start bond 1 before bond 2:

$$\sum_{p}^{n_{max}} z_{i,j-1,p} > \sum_{p}^{n_{max}} z_{i,j,p} \tag{17}$$

Eqs. (18)-(19) indicate that each functional group is attached to an existing and previous group:

$$z_{i,1,p} = \sum_{j}^{\upsilon_k} z_{p,j,i} \qquad i \in 2, 3, \ldots, n_{max} \tag{18}$$

$$z_{i,j,p} > z_{i,j+1,p+1} \qquad i \in 1, 2, \ldots, n_{max},$$
$$p \in 1, 2, \ldots, n_{max},\ j \in 2, \ldots, (S_{max} - 1) \tag{19}$$

Physical equilibrium

The amount of CO_2 in the liquid phase is determined by the physical equilibrium between the gas and liquid phases, which is defined by:

$$y_{CO_2} P \phi_{CO_2} = \gamma_{CO_2} P^{sat}_{CO_2} x_{CO_2} \tag{20}$$

where y_{CO_2} is the carbon dioxide mole fraction in the gas phase, P is the system pressure, ϕ_{CO_2} and γ_{CO_2} are the fugacity and activity coefficients, respectively, $P^{sat}_{CO_2}$ is the carbon dioxide vapor pressure and x_{CO_2} is the mole fraction in the liquid phase. Since ILs are characterized for featuring low vapor pressures, we may safely assume that the only compound in the gas phase is carbon dioxide, so $y_{CO_2} = 1$. Moreover, we also set the operating pressure at 3000 kPa. The remaining physical equilibrium model (Eq. (20)) is subject to the following constraints (Eqs. (21)–(39)).

Fugacity coefficient

The fugacity coefficient of carbon dioxide in the gas phase (ϕ_{CO_2}) was determined with the Peng-Robinson cubic equation of state (EOS), which in polynomial form is given by:

$$\ln \phi_{CO_2} = (Z_v - 1) - \ln(Z_v - B_z) - \frac{A_z}{2\sqrt{2}B_z} \ln\left(\frac{Z_v + 2.414B_z}{Z_v - 0.414B_z}\right) \tag{21}$$

where:

$$Z_v^3 + (B_z - 1)Z_v^2 + (A_z - 2B_z - 3B_z^2)Z_v + (B_z^3 + B_z^2 - A_z B_z) = 0 \tag{22}$$

$$A_z = \frac{0.4572 \alpha R^2 T_c^2 P}{R^2 T^2 P_c} \tag{23}$$

$$B_z = \frac{0.0778 R T_c P}{R T P_c} \tag{24}$$

$$\alpha = \left[1 + (0.3744 + 1.54226\omega - 0.26992\omega^2)(1 - T_r^{0.5})\right]^2 \tag{25}$$

$$T_r = T/T_c \tag{26}$$

Vapor pressure

The saturation pressure ($P^{sat}_{CO_2}$) was determined with the Antoine correlation (Perry et al., 1997):

$$P^{sat} = \exp\left(A_p + \frac{B_p}{T} + C_p \ln(T) + D_p T^{E_p}\right) \tag{27}$$

where A_p = 140.54, B_p = -4735.0, C_p = -21.268, D_p = 4.0909e-2 and E_p = 1 for carbon dioxide.

Activity coefficient

The UNIFAC group-contribution model was originally proposed in 1975 by Fredenslund et al. (1975) to predict liquid-phase activity coefficients in mixtures. In this method, the activity coefficient of component c (γ_c), which is expressed as a function of composition and temperature, is separated in two parts:

$$\ln \gamma_c = \ln \gamma_c^C + \ln \gamma_c^R \tag{28}$$

The first part, a combinatorial contribution ($\ln \gamma_c^C$), provides the contribution due to differences in molecular size and shape. The second part, a residual contribution ($\ln \gamma_c^R$), provides the contribution due to molecular interactions.

- Combinatorial contribution

  The combinatorial part of Eq. (28) can be obtained by:

$$\ln \gamma_c^C = 1 - Vi_c + \ln Vi_c - 5q_c\left(1 - \frac{Vi_c}{Fi_c} + \ln \frac{Vi_c}{Fi_c}\right) \tag{29}$$

$$Fi_c = \frac{q_c}{\sum_c q_c x_c} \tag{30}$$

$$Vi_c = \frac{r_c}{\sum_c r_c x_c} \tag{31}$$

$$q_c = \sum_k \nu k_k^c Q_k \tag{32}$$

$$r_c = \sum_k \nu k_k^c R_k \tag{33}$$

The parameters q_c and r_c are relative to molecular van der Waals volumes and molecular surface areas of the pure component and are calculated as the sum of the group volume (R_k) and group area (Q_k) parameters with Eqs. (32) and (33). Group parameters Q_k and R_k are normally obtained from van der Waals group volumes and surface areas. In this work such values were obtained from Dong et al. (2020a), http://www.

ddbst.com/published-parameters-unifac.html, Lei et al. (2009), Lei et al. (2012), Sander et al. (1983). Parameter νk_k^c represents the number of groups k in molecule c and is obtained by:

$$\nu k_k^c = \sum_i u_{i,k} \tag{34}$$

- Residual contribution
The residual part of Eq. (28) can be obtained by:

$$\ln \gamma_c^R = \sum_k \nu k_k^c \left(\ln \Gamma_k - \ln \Gamma_k^c\right) \tag{35}$$

where Γ_k is the group residual activity coefficient and Γ_k^c is the residual activity coefficient of group k in a reference solution that contains only molecules of type c.

$$\ln \Gamma_k = Q_k \left[1 - \ln\left(\sum_{k_1} \theta_{k_1} \psi_{k_1,k}\right) - \sum_{k_1} \frac{\theta_{k_1} \psi_{k,k_1}}{\sum_{k_2} \theta_{k_2} \psi_{k_2,k_1}}\right] \tag{36}$$

$$\theta_{k_1} = \frac{Q_{k_1} X_{k_1}}{\sum_{k_2} Q_{k_2} X_{k_2}} \tag{37}$$

$$X_{k_1} = \frac{\sum_c \nu k_{k_1}^c x_c}{\sum_c \sum_k \nu k_k^c x_c} \tag{38}$$

where X_{k_1} is the fraction of group k_1 in the mixture. The group interaction parameter ψ_{k_2,k_1} is defined by:

$$\psi_{k_2,k_1} = \exp(-a_{k_2,k_1}/T) \tag{39}$$

The parameter a_{k_2,k_1} characterizes the interaction between groups k_2 and k_1 and their values were taken from http://www.ddbst.com/published-parameters-unifac.html, Lei et al. (2009, 2012), Sander et al. (1983), Dong et al. (2020b), Nasirpour et al. (2020), Skjold-Jorgensen et al. (1979), Lei et al. (2014).

Physical properties

Pure ILs physical properties were determined by group-contribution methods, although not all bounds were considered as constraints, specifically density and viscosity. The molecular weight, critical volume, pressure and temperature, boiling temperature and density expressions (Eqs. (40)–(46)) were taken from Valderrama et al. (2012), while the melting temperature correlation (Eq. (47)) was obtained from Lazzús (2012) and the viscosity expression (Eq. (48)) was taken from Lazzús and Pulgar-Villarroel (2015).

- Molecular weight (MW):

$$MW = \sum_{i,k} u_{i,k} \Delta MW_k \tag{40}$$

- Critical volume (V_c):

$$V_c = 6.75 + \sum_{i,k} u_{i,k} \Delta V_{c_k} \tag{41}$$

- Critical temperature (T_c):

$$T_c = \frac{T_b}{0.5703 + 1.0121 \sum_{i,k} u_{i,k} \Delta T_{c_k} - \left(\sum_{i,k} u_{i,k} \Delta T_{c_k}\right)^2} \tag{42}$$

- Critical pressure (P_c):

$$P_c = \frac{MW}{\left(0.2573 + \sum_{i,k} u_{i,k} \Delta P_{c_k}\right)^2} \tag{43}$$

- Boling temperature (T_b):

$$T_b = 198.2 + \sum_{i,k} u_{i,k} \Delta T_{b_k} \tag{44}$$

- Density (ρ):

$$\rho = \left[0.01256 + 0.9533 \frac{MW}{V_c}\right]\left[\left(\frac{0.0039}{MW} + \frac{0.2987}{V_c}\right) V_c^{1.033}\right]^{\kappa} \tag{45}$$

where

$$\kappa = -\left[\frac{1 - T/T_c}{1 - T_b/T_c}\right]^{2/7} \tag{46}$$

- Melting temperature (T_m):

$$T_m = 288.7 + \sum_{i,k} u_{i,k} \Delta T_{m_k} \tag{47}$$

- Viscosity (η):

$$\ln \eta = 6.982 + \sum_{i,k} u_{i,k} \Delta \eta_{1_k} + \frac{\sum_{i,k} u_{i,k} \Delta \eta_{2_k}}{T} \tag{48}$$

The property bounds that were considered as constraints in this optimization problem are:

$$170 \le MW \le 800 \quad [=] \quad \text{g/gmol} \tag{49}$$

$$500 \le V_c \le 2000 \quad [=] \quad \text{cm}^3\text{/gmol} \tag{50}$$

$$910 \le T_c \le 1500 \quad [=] \quad \text{K} \tag{51}$$

$$10 \le P_c \le 50 \quad [=] \quad \text{bar} \tag{52}$$

$$450 \le T_b \le 1500 \quad [=] \quad \text{K} \tag{53}$$

$$253 \le T_m \le 298 \quad [=] \quad \text{K} \tag{54}$$

4.2. Ionic liquid mixture design

Objective function

The objective function for the ionic liquid mixture design problem is given by:

$$\max_{\mathbf{x_2},\mathbf{y_2}} \ \Omega_2 = x_{CO_2} \tag{55}$$

where x_{CO_2} is the carbon dioxide mole fraction in the liquid phase and $\mathbf{x_2}$ and $\mathbf{y_2}$ are the continuous and binary decision variables related to the MINLP problem.

Constraints

This optimization problem is subject to the same constraints involved in the pure ionic liquid design case (Section 4.1), that is, Eqs. (2)–(19) for the chemical structure of each IL, Eqs. (20)–(39) for the physical equilibrium between the liquid and gas phases, and Eqs. (49)–(54) for the IL physical properties bounds. It is important to highlight that the composition of each component in the liquid phase, explicitly found as x_c in Eqs. (30), (32) and (38), directly affects the activity coefficients and therefore the physical equilibrium. However, another constraint has to be included to account for each ionic liquid composition in the mixture.

Compositions summation

The composition of each ionic liquid, expressed in mole fraction (x_{IL_1} and x_{IL_2}), is obtained from Eq. (56):

$$\sum_c x_c = x_{CO_2} + x_{IL_1} + x_{IL_2} = 1 \tag{56}$$

Mixture properties

Even though the properties of the IL mixture were not considered as constraints, they were determined in order to estimate the mixtures properties. The molecular weight (MW_{mix}), as well as the boiling ($T_{b_{mix}}$) and melting ($T_{m_{mix}}$) temperatures of the IL mixture were obtained with the Kay mixing rules:

$$MW_{mix} = x_{IL_1} MW_{IL_1} + x_{IL_2} MW_{IL_2} \tag{57}$$

$$T_{b_{mix}} = x_{IL_1} T_{b_{IL_1}} + x_{IL_2} T_{b_{IL_2}} \tag{58}$$

$$T_{m_{mix}} = x_{IL_1} T_{m_{IL_1}} + x_{IL_2} T_{m_{IL_2}} \tag{59}$$

It is important to mention that Kay mixing rules are just an approximate way to compute mixture properties and naturally their use lead to some properties error.

The density of the IL mixture (ρ_{mix}) was determined using the following mixing rule (Lei et al., 2014):

$$\rho_{mix} = \frac{MW_{mix}}{\left(\frac{x_{IL_1} MW_{IL_1}}{\rho_{IL_1}} + \frac{x_{IL_2} MW_{IL_2}}{\rho_{IL_2}}\right)} \tag{60}$$

The viscosity of the IL mixture (η_{mix}) was obtained through the mixing rule proposed by Grunberg and Nissan (1949):

$$\log(\eta_{mix}) = x_{IL_1} \log \eta_{IL_1} + (1 - x_{IL_1}) \log(\eta_{IL_2}) \tag{61}$$

4.3. Separation process design

Objective function

The objective function to determine the optimal operation pressure and ionic liquid mixture feed stream conditions of a two stage absorption separation process is given by:

$$\max_{\mathbf{x_3}} \ \Omega_3 = \frac{V_{in} - V_{out}}{V_{in}} \tag{62}$$

where V_{in} and V_{out} are the CO_2 gas feed and outlet flow rates, respectively, and $\mathbf{x_3}$ are the continuous decision variables of this NonLinear Programming (NLP) problem. It should be stressed that in this step the chemical structure, as well as the mixture composition, of the ionic liquids were kept fixed.

Constraints

Since the chemical structure of each ionic liquid in the mixture, as well as the composition, were obtained in the previous optimization problem (Section 4.2), the resulting optimization problem is a NLP optimization problem subject to these three sets of constraints: (1) physical equilibrium between the liquid and gas phases in each, defined by Eqs. (20)–(39) at each equilibrium stage, (2) mass balance of the separation process described by Eqs. (63)–(66), and variable bounds defined by Eq. (67).

Mass balance

The absorption separation process has n_t stages and operates in a countercurrent flow manner, where the CO_2 gas inlet is feed in stage n_t+1, and the IL mixture is feed in stage 1. Since both ILs have a high boiling point, it is assumed that the only component present in the gas phase is CO_2 in any stage s ($y_{CO_2,s} = 1$). The mass balance of this process is given by:

- Stage 1:

$$L_{in} x_{c,in} + V_{s+1} y_{c,s+1} = L_s x_{c,s} + V_s y_{c,s} \tag{63}$$

- Stages 2 to n_t:

$$L_{s-1} x_{c,s-1} + V_{s+1} y_{c,s+1} = L_s x_{c,s} + V_s y_{c,s} \tag{64}$$

- Stage n_t+1:

$$L_{s-1} x_{c,s-1} + V_{in} y_{c,in} = L_s x_{c,s} + V_s y_{c,s} \tag{65}$$

- Liquid mole fraction summation in each stage:

$$\sum_c x_{c,s} = 1 \tag{66}$$

Variable bounds

The only variable bound considered in this NLP problem was the system temperature and was set to be at least 5 K higher than the IL melting temperatures bound:

$$303 \leq T \quad [=] \quad \text{K} \tag{67}$$

5. Results

In this section the results of this work are shown and discussed. We provide enough details to make an assessment of the scope and advantages of the proposed CAMD approach. First, the design of a single ionic liquid is addressed, followed by the design of mixtures of ionic liquids. Finally, single and two stages absorption processes are optimally designed, using an a priori synthesized ionic liquid mixture, to provide a numerical evidence about the advantages of using mixtures of ionic liquids for post-combustion CO_2 capture aims.

5.1. Pure ionic liquid design

For the pure ionic liquid CAMD problem, two different cases were analyzed. In the first one the chain of cations (–R in Fig. 2) attached to the anion-cation skeleton (elements 1 and 3 in Fig. 2) had to be a linear chain; in the second case, the chain could be nonlinear, that is, it could have ramifications. Interestingly, in both cases the resulting optimal IL molecular structure consisted of the same anion-cation skeleton, methyl imidazolium bis(trifluoromethylsulfonyl)-imide, but as defined earlier, different cations in the –R chain. The first one had a C_9 linear chain, one $-CH_3$ and eight $-CH_2$, whilst the nonlinear-chained IL resulted with three $-CH_3$, five $-CH_2$ and two -CH. Using the terminology exposed earlier, the resulting optimal ILs were [mIm][Tf_2N]-18 for the linear case and [mIm][Tf_2N]-352 for the nonlinear case. At 3000 kPa the CO_2 mole fraction absorbed by the linear-chained and nonlinear-chained IL were 0.3660 and 0.3819, respectively. The absorbed CO_2 by the later was slightly higher than the linear-chained one, which can be explained by the fact that the molecular structure has more cavities to capture CO_2. It has been reported that "absorptivity of CO_2 is determined in ILs primarily by electrostatic cation-anion interaction strengths; the larger the ions, the lower the ion density and the weaker the cation-anion attraction, which increases the amount of empty space and ease with which ions can be displaced to accommodate CO_2 between them" (Klahn and Seduraman, 2015). Regarding the resulting anion-cation skeleton, it has been stated (Ramdin et al., 2012) that generally ILs with a fluorine group have higher CO_2 solubility than those without a fluorine group and that CO_2 solubility increases as the number of fluorine groups in the anion increases, which endorses our resulting anion.

These two MINLP cases were also solved at different operating pressures. For both types of –R chains (linear and nonlinear), the resulting optimal IL molecular structures were always the same as in the 3000 kPa cases, but the amounts of absorbed CO_2 were significantly smaller as pressure decreased. Fig. 3 shows the CO_2 mole fraction captured by each ionic liquid at different pressures. Table 3 shows the MINLP statistics for the pure ionic liquid CAMD with linear and nonlinear -R chains.

To collect additional information, the pure IL CAMD problem was also solved to find the optimal –R chain, linear and nonlinear,

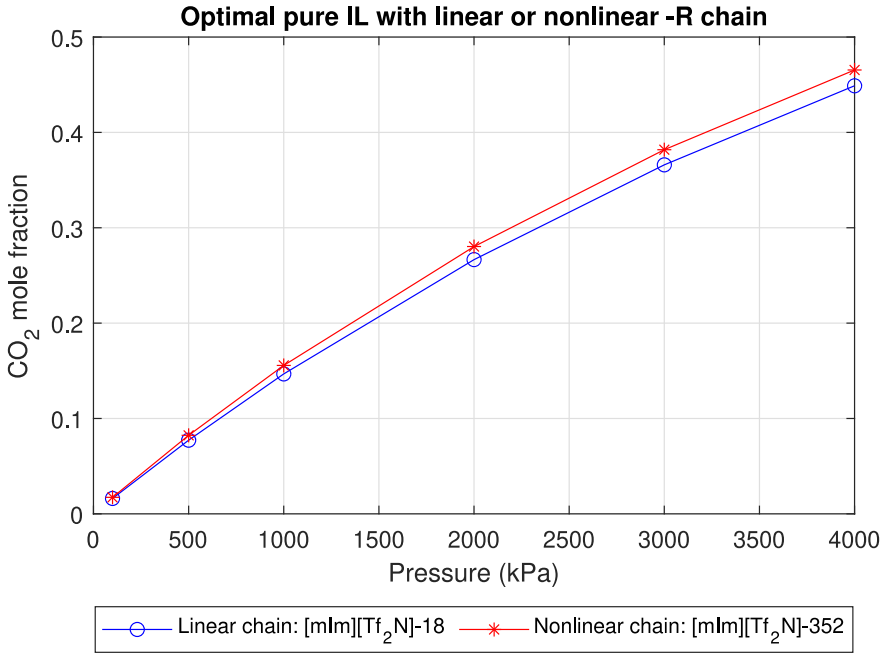

Fig. 3. Optimal pure ionic liquid CO_2 capture.

Table 3
MINLP statistics for the pure ionic liquid CAMD with linear and nonlinear -R chains.

Pressure (kPa)	CPU time (sec)	
	Linear chain	Nonlinear chain
100	4.265	7.597
500	4.576	6.707
1000	4.331	6.416
2000	4.331	6.416
3000	5.287	5.455
4000	5.952	4.080
5000	4.576	6.707
Single equations	1664	1663
Single variables	1892	1892
Discrete variables	758	758
Non zero elements	65,092	65,059
Non linear non zero elements	48,348	48,348

for each of the anion-cation skeletons in Table 1. It is important to mention that an optimal solution at 3000 kPa was found only for some of them. As shown in Table 4, the amount of captured CO_2 by these optimal ionic liquids is smaller than the one obtained with either [mIm][Tf_2N]-18 or [mIm][Tf_2N]-352, and in most cases, the IL with a nonlinear chain absorbs more CO_2 that the one with a linear chain. Of these ILs, the ones with the highest x_{CO_2} have the [mPy][Tf_2N] anion-cation skeleton, so it could be expected that the optimal IL mixture will have either the [mIm][Tf_2N] or the [mPy][Tf_2N] anion-cation skeleton.

5.2. Ionic liquid mixture design

The computation of the optimal CAMD IL mixture proved to be strongly dependent on the initial estimates of each IL physical properties, anion-cation skeleton and composition. This can be explained by the highly nonconvex and nonlinear nature of the optimization mathematical model. Several optimal IL mixtures were obtained, but only those with $x_{CO_2} > 0.3$, which resulted in 14 optimal mixtures (see Table 5), were selected. Table 5 shows the resulting mol fraction of each IL in a given optimal mixture. For example, optimal mixture 1 is composed of 0.579 [mIm][Tf_2N]-352 and 0.421 [mIm][Tf_2N]-11, and at the equilibrium, this mixture has 0.3681 CO_2 mol fraction. Since the approached MINLP is highly non-convex it turns out to be rather difficult to find a physical-based explanation regarding the optimal mixture composition. The CAMD problem consisted of 2571 single equations, 2718 single variables, 1516 discrete variables, 97,898 non zero elements and 65,419 nonlinear non zero elements. CPU usage times are included in Table 5. Although IL toxicity and biodegradability were not calculated, the optimal mixtures were classified based on their expected hazardousness according to their constituents, as presented by Abramenko et al. (2020). We used a color scheme to classify each cation-skeleton: red for the most-hazardous/least-biodegradable and green for the least-hazardous/most-biodegradable. So a red classification was used for the ILs that contained only [mIm] cation-skeletons, because it is the least biodegradable, while we used the green color for the ILs that contained only [mPy] cation-skeletons, because it is more biodegradable. For the mixtures, we applied the same color scheme and added the color blue to classify those mixtures that contained both types of anion-cation skeletons, denoting a medium biodegradability. As expected, in all mixtures one of the ionic liquid has the anion Tf_2N and the –352 chain. Furthermore, with the exception of only one case, both ionic liquids in the mixtures have the anion Tf_2N. Also as expected from the results obtained in the pure IL CAMD (Section 5.1), all mixtures have either the [mIm][Tf_2N] or the [mPy][Tf_2N] anion-cation skeleton.

Figs. 4 and 5 show various physical properties of the resulting optimal IL mixtures using the color scheme explained earlier. Fig. 4 shows the properties of mixtures in which one of the IL is [mIm][Tf_2N]-352 while Fig. 5 shows the properties of mixtures in which one IL is [mPy][Tf_2N]-352. For comparison purposes, in these two figures the corresponding pure IL properties were also included. A circle (•) was used to show the pure IL properties while a star (⋆) was used to show the IL mixture properties. In Fig. 4 it can be noticed that, even though the absorbed CO_2 is slightly lower in the mixtures with [mIm][Tf_2N]-352 than in the pure IL case, physical properties that are closely related to process operation, such as viscosity (Fig. 4(d)), are milder in the mixtures

Table 4
Optimal pure ionic liquids for each predefined anion-cation skeleton. CPU time in secs.

Anion-cation skeleton	Linear chain			Nonlinear chain		
	–R chain	x_{CO_2}	CPU time	–R chain	x_{CO_2}	CPU time
[mIm][Tf_2N]–	–18	0.3660	5.287	–352	0.3819	5.455
[mPy][Tf_2N]–	–15	0.3322	8.652	–352	0.3425	4.485
[mIm][$MeSO_4$]–	–16	0.2001	3.052	–16	0.2001	3.842
[mIm][TFA]–	–18	0.1413	3.842	–352	0.1582	4.146
[mIm][SCN]–	–19	0.0907	47.055	–271	0.0948	33.436
[mIm][$MDEGSO_4$]–	–19	0.0858	4.280	–19	0.0858	3.662
[mPyr][TfO]–	–09001	0.0808	36.786	–09001	0.0808	47.28
[mIm][$EtSO_4$]–	–19	0.0764	3.679	–0334	0.0451	9.075
[mIm][NO_3]–	–0901	0.0668	3.944	–0901	0.0668	3.353

Table 5
Carbon dioxide capture by different optimal ionic liquid mixtures, sorted by CO_2 mole fraction (x_{CO_2}).

Mix No.	x_{CO_2}	Ionic liquid 1		Ionic liquid 2		Mixture classification	CPU time (sec)
		Structure	x_{IL_1}	Structure	x_{IL_2}		
13	0.3796	[mIm][Tf_2N]-352	0.9848	[mIm][$MeSO_4$]-0301	0.0152	Red	11.715
6	0.3755	[mIm][Tf_2N]-352	0.7556	[mIm][Tf_2N]-12	0.2444	Red	22.194
1	0.3681	[mIm][Tf_2N]-352	0.5790	[mIm][Tf_2N]-11	0.4210	Red	16.247
7	0.3583	[mIm][Tf_2N]-352	0.4407	[mIm][Tf_2N]-1	0.5593	Red	30.337
11	0.3548	[mIm][Tf_2N]-352	0.4785	[mIm][Tf_2N]-0201	0.5215	Red	14.201
10	0.3542	[mIm][Tf_2N]-352	0.3639	[mPy][Tf_2N]-231	0.6361	Blue	33.102
8	0.3483	[mIm][Tf_2N]-352	0.3575	[mPy][Tf_2N]-15	0.6425	Blue	14.663
9	0.3453	[mIm][Tf_2N]-352	0.3061	[mPy][Tf_2N]-14	0.6939	Blue	20.320
12	0.3445	[mPy][Tf_2N]-352	0.7031	[mPy][Tf_2N]-1	0.2969	Green	21.560
5	0.3426	[mPy][Tf_2N]-352	0.5733	[mPy][Tf_2N]-12	0.4267	Green	21.441
14	0.3414	[mPy][Tf_2N]-352	0.4353	[mPy][Tf_2N]-11	0.5647	Green	13.693
2	0.3326	[mIm][Tf_2N]-352	0.3523	[mIm][Tf_2N]-0101	0.6477	Red	10.712
3	0.3196	[mIm][Tf_2N]-352	0.1383	[mPy][Tf_2N]-1	0.8617	Blue	12.403
4	0.3033	[mIm][Tf_2N]-352	0.2493	[mIm][Tf_2N]-0001	0.7507	Red	9.962

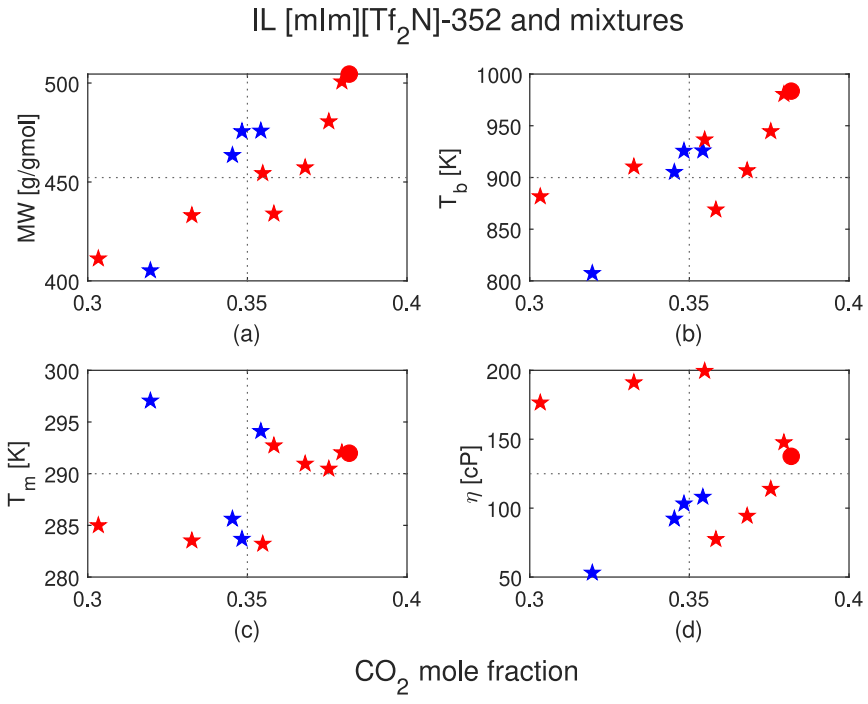

Fig. 4. Optimal ionic liquid mixtures with [mIm][Tf_2N]-352, where "●" denotes the pure IL, while "★" and "★" mixtures.

than in the pure IL case. A lower viscosity will reflect in lower pumping costs due to lower energy requirements. This is an advantage of using an IL mixture instead of a pure ionic liquid. Three of the mixtures (2, 4 and 11) resulted with viscosities higher than 150 cP and so were not included in the two-stage separation process calculations detailed in the next section.

Similarly, in Fig. 5 it can be observed that in the mixtures with [mPy][Tf_2N]-352 the CO_2 mole fraction is practically the same as in the pure IL case, and again, most physical properties are milder in the mixtures than in the pure IL case. As shown in Fig. 5(d), the pure IL viscosity is higher than 180 cP, which would result in operational difficulties, whilst the mixture viscosity is significantly

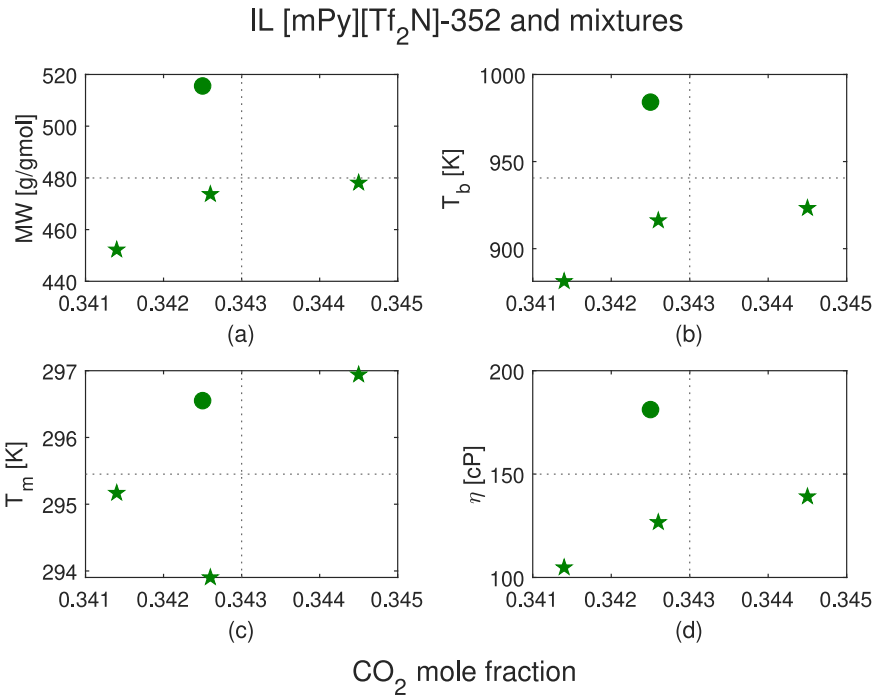

Fig. 5. Optimal ionic liquid mixtures with [mPy][Tf_2N]-352, where "●" denotes the pure IL and "★" mixtures.

Table 6
One stage separation process liquid and gas flow rates using different optimal ionic liquid mixtures, sorted by CO_2 % recovery.

Mixture No.	Liquid phase flow rate (gmol/min)	Gas phase flow rate (gmol/min)	CO_2 Recovery %	Mixture classification	CPU time (sec)
13	1,612.0	388.0	61.2	Red	0.377
6	1,601.4	398.6	60.1	Red	0.334
1	1,582.7	417.4	58.3	Red	0.292
7	1,558.4	441.6	55.8	Red	1.419
11	1,549.9	450.1	55.0	Red	0.376
10	1,548.5	451.5	54.9	Blue	0.338
8	1,534.5	465.5	53.5	Blue	0.366
9	1,527.4	472.6	52.7	Blue	0.364
12	1,525.6	474.4	52.7	Green	0.464
5	1,521.2	478.8	52.6	Green	0.447
14	1,518.3	481.7	52.1	Green	0.357
2	1,498.3	501.7	49.8	Red	0.431
3	1,469.7	530.3	47.0	Blue	0.371
4	1,435.4	564.6	43.5	Red	0.417

lower, which in return is favorable from the operational point of view.

5.3. Separation process design

The separation process design consisted of two cases. The first one, a one stage separation process, was a feasibility problem, with liquid and gas flow rates, and mol fraction of each component in the liquid phase as variables. The second case, a two stage separation process, was a NLP optimization problem with operating pressure and ionic liquid mixture feed stream as variables.

One stage process

For each of the mixtures obtained in Section 5.2, the amount of liquid and gas phase flow rates were determined for one equilibrium theoretical stage separation process at 303.15 K and 3000 kPa, with a liquid phase feed stream of 1000 gmol/min of IL mixture and a gas phase flow stream of 1000 gmol/min of CO_2 pure gas. The recovery rate (see Table 6) varies between 44% and 61%, and in the best case (mixture 13), the amount of captured CO_2 is 612 gmol/min, practically 40% higher than the amount captured in the worst case (mixture 4) with 435 gmol/min. This NLP problem had between 116 and 164 single variables and equations, between 896 and 2014 non zero elements and between 788 and 1868 non linear non zero elements. Table 6 shows the CPU usage time.

Multiple stage process

For ILs mixtures with a viscosity lower than 150 cP, the optimal ionic liquid mixture feed stream was determined for a two equilibrium stage separation process at different operation pressures. In these NLP problems, the gas feed stream (V_{in}) was fixed at 1000 gmol/min. Only two stages were used because in all cases 100% CO_2 recovery was achieved. Fig. 6(a) shows the mixtures with [mIm][Tf_2N]-352, whilst Fig. 6(b) shows the ILs mixture feed stream for mixtures featuring [mPy][Tf_2N]-352. In these cases, at high pressures the amount of ionic liquid mixture feed stream is practically the same, but as pressure decreases, the amount of IL feed stream is higher in the mixtures than in the pure IL cases.

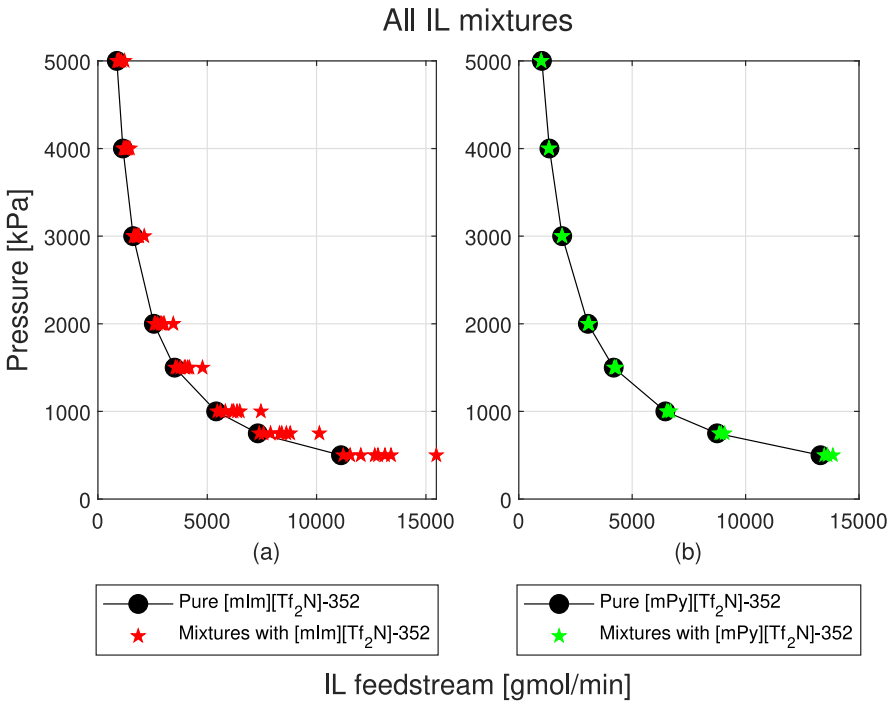

Fig. 6. IL feed stream for optimal mixtures in a two stage separation process at different pressures.

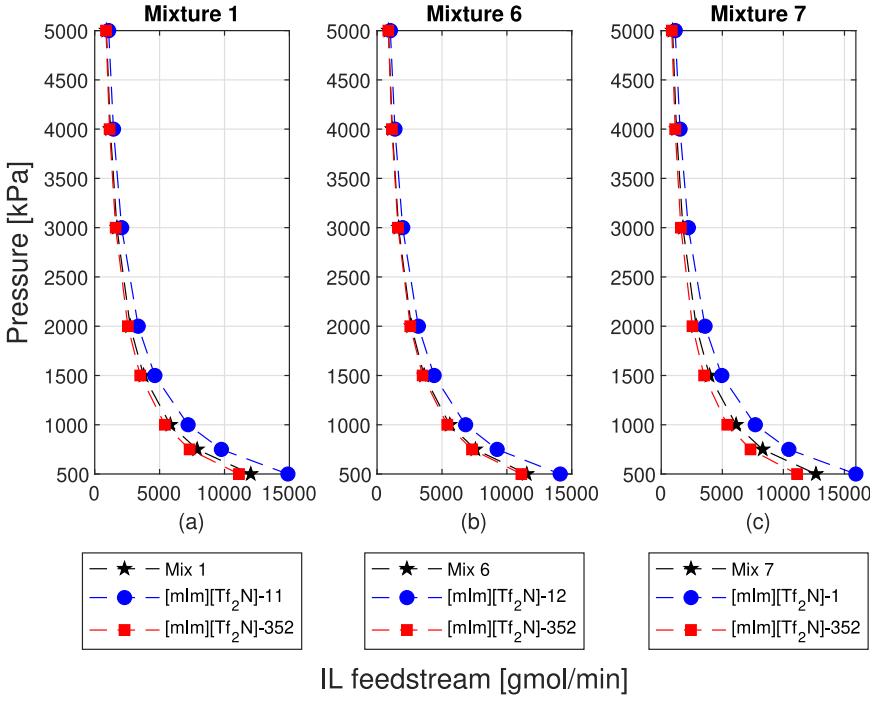

Fig. 7. IL feed stream in a two stage separation process at different pressures for mixtures where both ILs have [mIm][Tf_2N] skeletons.

Fig. 7 shows these results for mixtures where both ILs have [mIm][Tf_2N] skeletons, Fig. 8 for the one mixture that has [mIm][Tf_2N] and [mIm][$MeSO_4$] skeletons, Fig. 9 for mixtures with both [mIm][Tf_2N] and [mPy][Tf_2N] skeletons and, lastly, Fig. 10 shows the results for those mixtures where both ILs have [mPy][Tf_2N] skeletons.

The best operating conditions for a given ILs mixture are those with the lowest operating pressure and the lowest IL feed stream. However, these two variables change in opposite directions: the lowest pressure is met at the highest feed stream, and vice versa. So there has to be a compromise, the optimal operation conditions have to be somewhere in the middle. This point can be determined from the Pareto graph. Hence, the best operating point is located along the solution curve which is closest to the utopia point. The utopia point is the intersection between the extension of each end on the solution curve, and the distance between the utopia point and the solution curve can be determined by the Euclidian norm.

In Fig. 11 we illustrate these calculations for ILs mixture 10, where the utopia point is given by $P = 1{,}102.7$ kPa and $L_{in} = 2{,}197.9$ gmol/min (shown by a blue dot) and the optimal conditions are

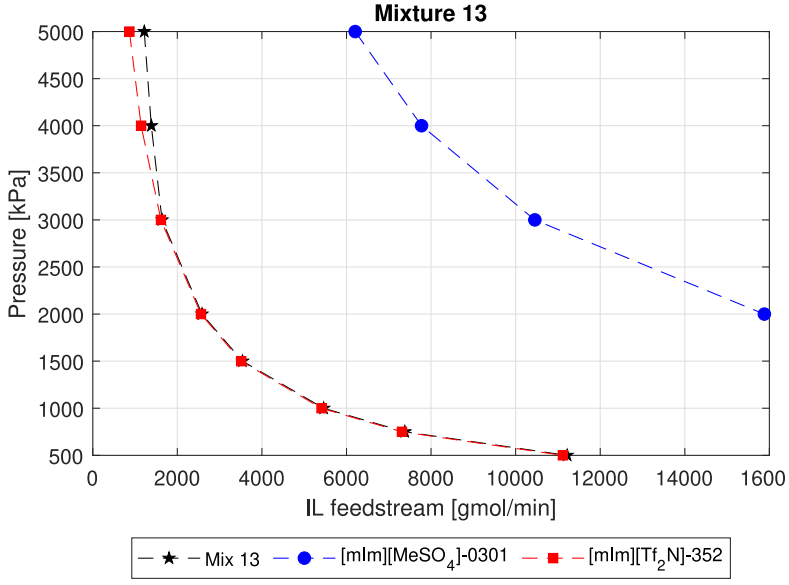

Fig. 8. IL feed stream in a two stage separation process at different pressures for the mixture with [mIm][Tf_2N] and [mIm][$MeSO_4$] skeletons.

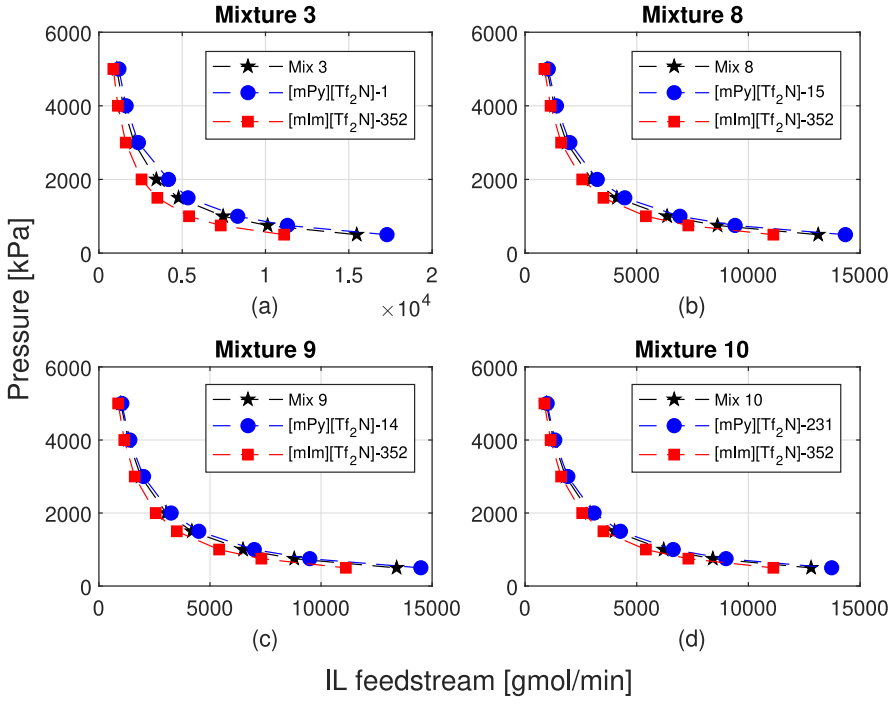

Fig. 9. IL feed stream in a two stage separation process at different pressures for mixtures with both [mIm][Tf_2N] and [mPy][Tf_2N] skeletons.

then given by $P = 2{,}062.5$ kPa and $L_{in} = 2{,}809.4$ gmol/min (shown in Fig. 11 with a red star). These calculations were done for the ILs mixtures that had a viscosity lower than 150 cP and are presented in Table 7. Additional Pareto graphs for each ILs mixture presented in Table 7 can be found in the Supplementary Material section.

Optimal pressure and liquid feed stream for studied mixtures (Table 7) have similar values: pressures are practically the same, between 2000 and 2150 kPa, and ionic liquid mixture feeds are in a close range, between 2600 and 3200 gmol/min. This can be explained by the fact that all mixtures have one ionic liquid with the same anion ([Tf_2N]) and chain (–$(CH)_2(CH_2)_5(CH_3)_3$) and, as shown in Fig. 6, the optimal pressure vs. optimal IL feed plots are practically the same. These results indicate that the operation pressure

Table 7
Optimal IL feed stream and operation pressure for ILs mixtures.

Mixture No.	Optimal liquid feed stream (L_{in}, gmol/min)	Optimal operating pressure (P, kPa)
13	2,582.0	2,000.8
6	2,618.6	2,014.2
1	2,683.4	2,034.3
7	2,773.9	2,057.9
10	2,810.9	2,061.5
8	2,865.7	2,072.4
9	2,896.2	2,082.7
12	2,905.6	2,084.1
5	2,925.1	2,088.7
14	2,938.9	2,098.5
3	3,176.2	2,144.7

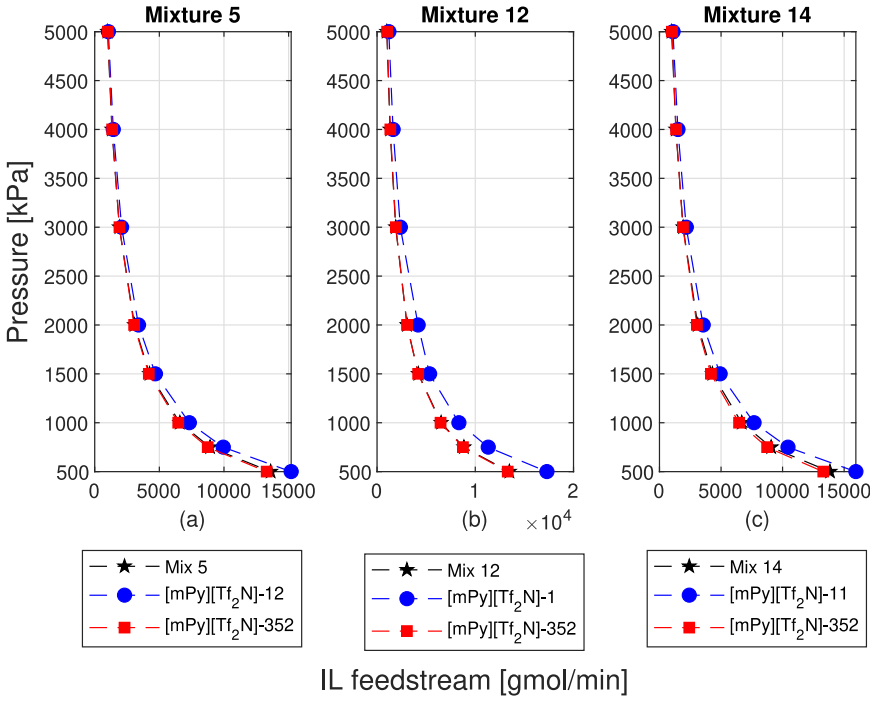

Fig. 10. IL feed stream in a two stage separation process at different pressures for mixtures where both IL have [mPy][Tf_2N] skeletons.

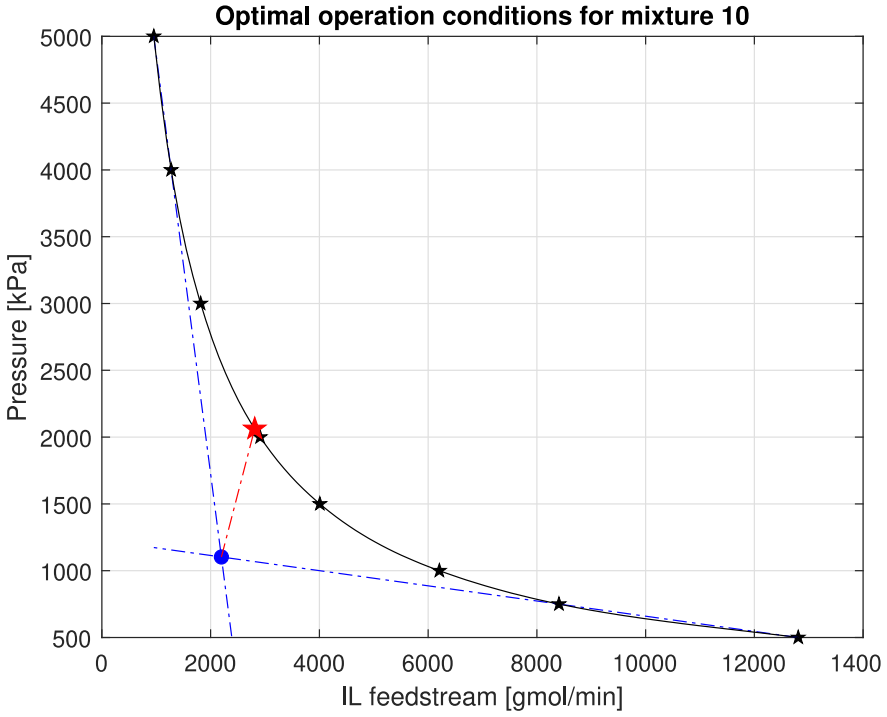

Fig. 11. Optimal operation conditions for ILs mixture No. 10, where "●" denotes the utopia point and "★" denotes the optimal operation conditions.

of the apsorption process will be 20 bars, so the CO_2 gas inlet will have to be also at that pressure.

6. Conclusions and future work

In this work the post-combustion carbon dioxide capture capabilities of optimally designed ionic liquids and its mixtures where addressed. The resulting optimal ILs mixtures had either [mIm][Tf_2N]-352 or [mPy][Tf_2N]-352, being [mIm][Tf_2N]-352 the optimal pure ionic liquid. The carbon dioxide mole fraction in a one stage separation process was higher when using a pure IL, but it was not significantly higher than the one achieved with the ILs mixture. As to the operation conditions, no major difference was found between the use of pure IL or their mixtures. Using ILs mixtures instead of pure IL for CO_2 capture can be favorable from the operational point of view since most of the physical properties of the mixture are milder without loosing much CO_2 absorption capacity. Furthermore, if we take into consideration the expected hazardousness of an IL based on its constituents, an ILs mixture may be a better choice for CO_2 capture as it may be more envi-

ronmentally friendly (less hazardous and more biodegradable). So if we base our selection merely on the CO_2 solubility, our selection may not be the best operationally or environmentally.

Several things can be done to advance this work, such as include N_2 and other gases in the gas phase stream, use machine learning to predict CO_2 solubility and related physical and thermodynamic properties, incorporate uncertainty in the estimation of properties, calculate toxicity or biodegradability, expand the ions used, validate our results with experimental data and include the energy balance. Currently we are expanding this work by including nitrogen in the gas stream, since we worked with a pure CO_2 feed stream, and using machine learning to estimate CO_2 solubility instead of using activity coefficients.

Declaration of Competing Interest

On behalf of my co-authors and myself, we declare no conflict of interest regarding our common research work: “Optimal Computer-Aided Molecular Design of Ionic Liquid Mixtures for Post-Combustion Carbon Dioxide Capture”.

Supplementary material

Supplementary material associated with this article can be found, in the online version, at doi:10.1016/j.compchemeng.2021.107622.

CRediT authorship contribution statement

Andrea Silva-Beard: Methodology, Software, Validation, Formal analysis, Investigation, Resources, Data curation, Writing – original draft, Writing – review & editing, Visualization. **Antonio Flores-Tlacuahuac:** Conceptualization, Methodology, Software, Validation, Formal analysis, Investigation, Resources, Data curation, Writing – original draft, Writing – review & editing, Visualization, Supervision. **Martín Rivera-Toledo:** Conceptualization, Methodology, Formal analysis, Resources, Data curation, Writing – review & editing, Supervision.

References

Abramenko, N., Kustov, L., Metelytsia, L., Kovalishyn, V., Tetko, I., Peijnenburg, W., 2020. A review of recent advances towards the development of QSAR models for toxicity assessment of ionic liquids. J. Hazard. Mater. 384, 121429.

Aghaie, M., Rezaei, N., Zendehboudi, S., 2018. A systematic review on CO_2 capture with ionic liquids: current status and future prospects. Renew. Sustain. Energy Rev. 96, 502–525.

Austin, N.D., Sahinidis, N.V., Trahan, D.W., 2016. Computer-aided molecular design: an introduction and review of tools, applications, and solution techniques. Chem. Eng. Res. Des. 116, 2–26.

Avila, J., Lepre, L.F., Santini, C.C., Tiano, M., Denis-Quanquin, S., Chung Szeto, K., Padua, A.A., Costa Gomes, M., 2021. High-performance porous ionic liquids for low-pressure CO_2 capture. Angew. Chem. Int. Ed. 60 (23), 12876–12882.

Chemmangattuvalappil, N.G., Ng, D.K., Ng, L.Y., Ooi, J., Chong, J.W., Eden, M.R., 2020. A review of process systems engineering (PSE) tools for the design of ionic liquids and integrated biorefineries. Processes 8 (12), 1678.

Chen, Y., Gani, R., Kontogeorgis, G.M., Woodley, J.M., 2019. Integrated ionic liquid and process design involving azeotropic separation processes. Chem. Eng. Sci. 203, 402–414.

Chen, Y., Koumaditi, E., Gani, R., Kontogeorgis, G.M., Woodley, J.M., 2019. Computer-aided design of ionic liquids for hybrid process schemes. Comput. Chem. Eng. 130, 106556.

Chen, Y., Woodley, J., Kontogeorgis, G., Gani, R., 2018. Integrated ionic liquid and process design involving hybrid separation schemes. In: Eden, M.R., Ierapetritou, M.G., Towler, G.P. (Eds.), 13th International Symposium on Process Systems Engineering (PSE 2018). In: Computer Aided Chemical Engineering, Vol. 44. Elsevier, pp. 1045–1050.

Chong, F.K., Andiappan, V., Ng, D.K., Foo, D.C., Eljack, F.T., Atilhan, M., Chemmangattuvalappil, N.G., 2017. Design of ionic liquid as carbon capture solvent for a bioenergy system: integration of bioenergy and carbon capture systems. ACS Sustain. Chem. Eng. 5 (6), 5241–5252.

Chong, F.K., Foo, D.C., Eljack, F.T., Atilhan, M., Chemmangattuvalappil, N.G., 2016. A systematic approach to design task-specific ionic liquids and their optimal operating conditions. Mol. Syst. Des. Eng. 1 (1), 109–121.

Churi, N., Achenie, L.E., 1996. Novel mathematical programming model for computer aided molecular design. Ind. Eng. Chem. Res. 35 (10), 3788–3794.

Dong, Y., Guo, Y., Zhu, R., Zhang, J., Lei, Z., 2020. UNIFAC model for ionic liquids. 2. Revision and extension. Ind. Eng. Chem. Res..

Dong, Y., Huang, S., Guo, Y., Lei, Z., 2020. COSMO-UNIFAC model for ionic liquids. AIChE J. 66 (1), e16787.

Fredenslund, A., Jones, R.L., Prausnitz, J.M., 1975. Group-contribution estimation of activity coefficients in nonideal liquid mixtures. AIChE J. 21 (6), 1086–1099.

Gani, R., 2004. Chemical product design: challenges and opportunities. Comput. Chem. Eng. 28 (12), 2441–2457.

Georgiadis, M.C., Schenk, M., Pistikopoulos, E.N., Gani, R., 2002. The interactions of design control and operability in reactive distillation systems. Comput. Chem. Eng. 26 (4–5), 735–746.

Grunberg, L., Nissan, A.H., 1949. Mixture law for viscosity. Nature 164 (4175), 799–800.

Gurkan, B., Goodrich, B., Mindrup, E., Ficke, L., Massel, M., Seo, S., Senftle, T., Wu, H., Glaser, M., Shah, J., et al., 2010. Molecular design of high capacity, low viscosity, chemically tunable ionic liquids for CO_2 capture. J. Phys. Chem. Lett. 1 (24), 3494–3499.

Hada, S., Herring, R.H., Davis, S.E., Eden, M.R., 2015. Multivariate characterization, modeling, and design of ionic liquid molecules. Comput. Chem. Eng. 81, 310–322.

Hospital-Benito, D., Lemus, J., Moya, C., Santiago, R., Palomar, J., 2020. Process analysis overview of ionic liquids on CO_2 chemical capture. Chem. Eng. J. 390, 124509.

Karunanithi, A.T., Mehrkesh, A., 2013. Computer-aided design of tailor-made ionic liquids. AIChE J. 59 (12), 4627–4640.

Klahn, M., Seduraman, A., 2015. What determines CO_2 solubility in ionic liquids? A molecular simulation study. J. Phys. Chem. B 119 (31), 10066–10078.

Lazzús, J.A., 2012. A group contribution method to predict the melting point of ionic liquids. Fluid Phase Equilib. 313, 1–6.

Lazzús, J.A., Pulgar-Villarroel, G., 2015. A group contribution method to estimate the viscosity of ionic liquids at different temperatures. J. Mol. Liq. 209, 161–168.

Lei, Z., Chen, B., Koo, Y.-M., MacFarlane, D.R., 2017. Introduction: ionic liquids. Chem. Rev. 117 (10), 6633–6635.

Lei, Z., Dai, C., Liu, X., Xiao, L., Chen, B., 2012. Extension of the UNIFAC model for ionic liquids. Ind. Eng. Chem. Res. 51 (37), 12135–12144.

Lei, Z., Dai, C., Wang, W., Chen, B., 2014. UNIFAC model for ionic liquid-CO_2 systems. AIChE J. 60 (2), 716–729.

Lei, Z., Zhang, J., Li, Q., Chen, B., 2009. UNIFAC model for ionic liquids. Ind. Eng. Chem. Res. 48 (5), 2697–2704.

López-Bautista, L.A., Flores-Tlacuahuac, A., 2020. Optimization of the amines-CO_2 capture process by a nonequilibrium rate-based modeling approach. AIChE J. 66 (6), e16978.

Lotto, M.A., Nabity, J.A., Klaus, D.M., 2021. Low-pressure CO_2 capture using ionic liquids to enable mars propellant production. J. Propul. Power 37 (1), 100–107.

MacFarlane, D.R., Tachikawa, N., Forsyth, M., Pringle, J.M., Howlett, P.C., Elliott, G.D., Davis, J.H., Watanabe, M., Simon, P., Angell, C.A., 2014. Energy applications of ionic liquids. Energy Environ. Sci. 7 (1), 232–250.

Molina-Thierry, D.P., Flores-Tlacuahuac, A., 2015. Simultaneous optimal design of organic mixtures and rankine cycles for low-temperature energy recovery. Ind. Eng. Chem. Res. 54 (13), 3367–3383.

Mortazavi-Manesh, S., Satyro, M., Marriott, R.A., 2011. A semi-empirical Henry's law expression for carbon dioxide dissolution in ionic liquids. Fluid Phase Equilib 307 (2), 208–215.

Murphy, K.P., 2012. Machine Learning: A Probabilistic Perspective. MIT press.

Nasirpour, N., Mohammadpourfard, M., Heris, S.Z., 2020. Ionic liquids: promising compounds for sustainable chemical processes and applications. Chem. Eng. Res. Des. 160, 264–300.

Niedermeyer, H., Hallett, J.P., Villar-Garcia, I.J., Hunt, P.A., Welton, T., 2012. Mixtures of ionic liquids. Chem. Soc. Rev. 41 (23), 7780–7802.

Palomar, J., Larriba, M., Lemus, J., Moreno, D., Santiago, R., Moya, C., De Riva, J., Pedrosa, G., 2019. Demonstrating the key role of kinetics over thermodynamics in the selection of ionic liquids for CO_2 physical absorption. Sep. Purif Technol. 213, 578–586.

Perry, R., Green, D., Maloney, J., 1997. Chemical Engineers' Handbook Seventh Edition. McGraw-Hill.

Plechkova, N.V., Seddon, K.R., 2008. Applications of ionic liquids in the chemical industry. Chem. Soc. Rev. 37 (1), 123–150.

Rahman, F.A., Aziz, M.M.A., Saidur, R., Bakar, W.A.W.A., Hainin, M., Putrajaya, R., Hassan, N.A., 2017. Pollution to solution: capture and sequestration of carbon dioxide (CO_2) and its utilization as a renewable energy source for a sustainable future. Renew. Sustain. Energy Rev. 71, 112–126.

Ramdin, M., de Loos, T.W., Vlugt, T.J., 2012. State-of-the-art of CO_2 capture with ionic liquids. Ind. Eng. Chem. Res. 51 (24), 8149–8177.

Ramsundar, B., Eastman, P., Walters, P., Pande, V., 2019. Deep Learning for the Life sciences: Applying Deep Learning to Genomics, Microscopy, Drug Discovery, and More. O'Reilly Media, Inc..

de Riva, J., Suarez-Reyes, J., Moreno, D., Díaz, I., Ferro, V., Palomar, J., 2017. Ionic liquids for post-combustion CO_2 capture by physical absorption: thermodynamic, kinetic and process analysis. Int. J. Greenhouse Gas Control 61, 61–70.

Sakizlis, V., Perkins, J.D., Pistikopoulos, E.N., 2004. Recent advances in optimization-based simultaneous process and control design. Comput. Chem. Eng. 28 (10), 2069–2086.

Sander, B., Skjold-Jørgensen, S., Rasmussen, P., 1983. Gas solubility calculations. I. UNIFAC. Fluid Phase Equilib. 11 (2), 105–126.

Seddon, K.R., 1997. Ionic liquids for clean technology. J. Chem. Technol. Biotechnol. 68 (4), 351–356.
Senftle, T.P., Carter, E.A., 2017. The holy grail: chemistry enabling an economically viable CO_2 capture, utilization, and storage strategy. Acc. Chem. Res. 50 (3), 472–475.
Seo, K., Tsay, C., Hong, B., Edgar, T.F., Stadtherr, M.A., Baldea, M., 2020. Rate-based process optimization and sensitivity analysis for ionic-liquid-based post-combustion carbon capture. ACS Sustain. Chem. Eng. 8 (27), 10242–10258.
Sistla, Y.S., Khanna, A., 2014. Carbon dioxide absorption studies using amine-functionalized ionic liquids. J. Ind. Eng. Chem. 20 (4), 2497–2509.
Skjold-Jorgensen, S., Kolbe, B., Gmehling, J., Rasmussen, P., 1979. Vapor-liquid equilibria by UNIFAC group contribution. revision and extension. Ind. Eng. Chem. Process Des. Dev. 18 (4), 714–722.
Sreedhar, I., Nahar, T., Venugopal, A., Srinivas, B., 2017. Carbon capture by absorption–path covered and ahead. Renew. Sustain. Energy Rev. 76, 1080–1107.
Taheri, M., Dai, C., Lei, Z., 2018. CO_2 capture by methanol, ionic liquid, and their binary mixtures: experiments, modeling, and process simulation. AlChE J. 64 (6), 2168–2180.
Torralba-Calleja, E., Skinner, J., Gutiérrez-Tauste, D., 2013. CO_2 capture in ionic liquids: a review of solubilities and experimental methods. J. Chem. 2013.
Valderrama, J.O., Forero, L.A., Rojas, R.E., 2012. Critical properties and normal boiling temperature of ionic liquids. update and a new consistency test. Ind. Eng. Chem. Res. 51 (22), 7838–7844.
Valencia-Marquez, D., Flores-Tlacuahuac, A., García-Cuéllar, A.J., Ricardez-Sandoval, L., 2021. Computer aided molecular design coupled with molecular dynamics as a novel approach to design new lubricants. Comput. Chem. Eng. 107523.
Valencia-Marquez, D., Flores-Tlacuahuac, A., Vasquez-Medrano, R., 2011. Simultaneous optimal design of an extractive column and ionic liquid for the separation of bioethanol–water mixtures. Ind. Eng. Chem. Res. 51 (17), 5866–5880.
Valencia-Marquez, D., Flores-Tlacuahuac, A., Vasquez-Medrano, R., 2017. An optimization approach for CO_2 capture using ionic liquids. J. Clean. Prod. 168, 1652–1667.
Zhang, L., Mao, H., Liu, Q., Gani, R., 2020. Chemical product design–recent advances and perspectives. Curr. Opin. Chem. Eng. 27, 22–34.
Zhang, X., Ding, X., Song, Z., Zhou, T., Sundmacher, K., 2021. Integrated ionic liquid and rate-based absorption process design for gas separation: global optimization using hybrid models. AlChE J. 67 (10), e17340.
Zhang, X., Wang, J., Song, Z., Zhou, T., 2021. Data-driven ionic liquid design for CO_2 capture: molecular structure optimization and DFT verification. Ind. Eng. Chem. Res. 60 (27), 9992–10000.
Zhang, X., Zhang, X., Dong, H., Zhao, Z., Zhang, S., Huang, Y., 2012. Carbon capture with ionic liquids: overview and progress. Energy Environ. Sci. 5 (5), 6668–6681.
Zhou, T., Shi, H., Ding, X., Zhou, Y., 2021. Thermodynamic modeling and rational design of ionic liquids for pre-combustion carbon capture. Chem. Eng. Sci. 229, 116076.